

Individual heterogeneity in the functional topography of the default-mode network in medial prefrontal cortex

Claudio Toro-Serey, Sean Tobyne, & Joseph T. McGuire

1. Department of Psychological and Brain Sciences, Boston University, Boston, USA

Corresponding author:

Abstract

There is extensive topographic overlap between cortical regions associated with the default-mode network (DMN) and regions that exhibit effects of subjective value during decision making. The two sets of functional effects involve common regions of medial prefrontal cortex (mPFC) and posterior cingulate cortex (PCC). At the same time, differences between the two sets of activation patterns are not apparent at the aggregated meta-analytic level, and further individual-level functional subdivisions might be obscured by group averaging. Here we used cortical surface-based meta-analysis to identify a parcel in human PCC that was preferentially implicated in DMN effects. We then used resting-state fMRI data and a data-driven network analysis algorithm, spectral partitioning, to divide mPFC/PCC into distinct cortical communities in individual participants ($n = 100$ from the Human Connectome Project). We labeled the communities “DMN” and “non-DMN” on the basis of their overlap with the meta-analytically identified PCC region. The spectral partitioning algorithm efficiently identified individual-level cortical subdivisions that were reliable over time and across test-retest days using moderate amounts of fMRI data (30 min per day). The topography of the identified subdivisions differed across individuals, and the degree of inter-individual variability was greater in mPFC than in PCC. Our results will aid future task-based fMRI studies in identifying functionally specific cortical subdivisions, and suggest it would be premature to infer that different task manipulations call upon shared cognitive processes solely because they evoke overlapping activation in mPFC at the group or meta-analytic level.

Keywords: brain networks; DMN; individual differences

Introduction

Human medial prefrontal cortex (mPFC) and posterior cingulate cortex (PCC) are jointly associated with a large set of disparate cognitive functions (Hiser and Koenigs 2018; Kragel et al. 2018), including the subjective value (SV) assigned to decision outcomes (Bartra, McGuire, and Kable 2013; Clithero and Rangel 2014; Hiser and Koenigs 2018; Kable and Glimcher 2007; Levy et al. 2011). Choice-related activity in these areas has shown significant spatial overlap with the default mode network (DMN) along the medial wall (M. D. Fox et al. 2005; Laird et al. 2009; Yeo et al. 2011), prompting the question of whether (and to what extent) these two systems can be dissociated.

Previous coordinate-based meta-analyses have identified topographically similar activation patterns in mPFC for valuation (Bartra, McGuire, and Kable 2013; Clithero and Rangel 2014) and default-mode task deactivation (Laird et al. 2009). More focused meta-analytic work aimed at disentangling DMN from subjective value has determined that these systems are inseparable within mPFC (Acikalin, Gorgolewski, and Poldrack 2017), even though there is clear divergence in other areas (ventral striatum in favor of SV, with DMN exclusively on sections of PCC and the temporoparietal junction). These findings highlight the multifaceted embedding of psychological constructs in subregions of mPFC, and suggest that DMN and valuation might indeed be subserved by the same neural system.

A key limitation of group-averaging and meta-analysis is that individual-specific functional subdivisions can be overlooked. Averaging has traditionally been beneficial in identifying tendencies in brain function and organization when faced with short scanning sessions per subject. However, it has been shown that mPFC is subject to considerable idiosyncratic cortical folding (Zilles, Palomero-Gallagher, and Amunts 2013; Mackey and Petrides 2014) and inter-subject functional variability (Mueller et al. 2013), thus making group-averaging studies difficult to interpret.

Seeking to remedy these shortcomings, recent work has prescribed relevance to the analysis of single subjects in fMRI. Individual analyses of fMRI data have identified idiosyncratic, reliable, and valid functional organization that would otherwise be blurred in aggregative estimations (T. O. Laumann et al. 2015; Gordon et al. 2017; Gratton et al. 2018; Tobyne et al. 2018). Furthermore, subject-specific network arrangements have been found to predict behavioral characteristics (Kong et al. 2018). In regards to DMN, the trend of individualized analyses has led to finer idiosyncratic subdivisions of the DMN through careful selection of seed-based functional connectivity (Braga and Buckner 2017). It is thus possible that the indistinguishable overlap of DMN and valuation effects can be attributed to a lack of spatial resolution that is better understood at the individual level. With this in mind, an important first step in disentangling these phenomena would be to

determine the degree of topological heterogeneity of the DMN present within mPFC.

Interrogating all sources of covariation through functional connectivity provides an avenue for capturing subject-specific brain organization. Connectome-based analyses of resting state functional connectivity (rsFC) have been fruitful in characterizing individualized functional topologies that match task-induced activity (Gordon et al. 2017; T. O. Laumann et al. 2015; Tobyne et al. 2017). A popular approach to analyze these connectomes is to rely on graph theoretic methods, which are properly equipped to understand brain network dynamics (D. S. Bassett, Zurn, and Gold 2018). From these, community detection algorithms have been successfully utilized to section brain networks into cohesive substructures (Garcia et al. 2017). Such communities represent clusters of network nodes that are more connected with each other than with the rest of the network (Fortunato and Hric 2016). Among the algorithms used to estimate these communities, modularity has been widely effective in subsectioning brain networks into multiple groups (Garcia et al. 2017). However, in attempting to refine the DMN topology at the individual level, dividing these regions into what belongs and does not belong to DMN makes a forced dissection through spectral partitioning (SP) a more valuable option (Fiedler 1975; Belkin and Niyogi 2003). SP has recently been used to characterize the posterior-anterior functional gradient of the insula using rsfMRI data (Tian and Zalesky 2018). This method can thus capture a refined group of brain regions that more cohesively share activation patterns during rest.

In this study, we aimed to subsection regions commonly attributed to both DMN and subjective value into subject-specific DMN and non-DMN partitions, quantifying the degree of topographical heterogeneity present in this network within and across individuals. We did this by capitalizing on the respective strengths of meta-analytic and subject-specific analyses of brain networks. First, we established a search space by selecting parcels from an established brain atlas (M. F. Glasser et al. 2016) that considerably overlapped with previously-defined DMN and limbic networks along the medial wall (Yeo et al. 2011). A meta-analysis of DMN and SV literatures revealed areas in PCC and mPFC that were uniquely related to DMN and SV, respectively (these areas were used as markers to identify the affiliation of each individual's communities). We then produced rsFC networks of all the surface vertices within these regions of interest (ROI) for each of 100 individual resting state dataset from the Human Connectome Project (HCP)(Van Essen et al. 2012), and estimated the extent of DMN coverage through spectral partitioning. Focusing on individual vertices in this search space rather than the parcels (as is usual in brain network analyses) allowed us to finely delineate the topographical extent of each community. We found that these areas of overlap can be partitioned into two communities that topographically vary across subjects, but that follow a common organizational principle. This partition was in substantial agreement with results from a different community detection algorithm (modularity). A sliding window analysis showed that spectral partitioning allows for a more

immediate identification of noisy vertices with unreliable affiliation. Refining the partitions by filtering out these nodes resulted in idiosyncratic partitions that were highly stable across scanning runs per individual, and this pattern was higher for mPFC. We show that partitions produced by spectral partitioning had higher test-retest reliability per subject than common seed-based functional connectivity, without the need of group-driven priors (Kong et al. 2018). Lastly, we provide evidence that these communities resembled an organizational scheme recently observed in a handful of subjects (Braga and Buckner 2017). Our work highlights the usefulness of estimating brain effects at the individual level in these regions, and points to limitations of aggregative methods in determining the degree of neural overlap between DMN and valuation.

Methods

Search space

For all our analyses, we defined our search space based on the 17 network parcellation proposed by Yeo et al. (2011). First, We selected vertices on the cortical surface that were contained by the DMN and limbic networks along the medial wall. Next, we overlayed these networks on a parcellated atlas of the human cortical surface (360 regions) (M. F. Glasser et al. 2016), and retained parcels that shared a considerable amount of vertices with them (visually inspected). This resulted in 45 regions of interest (ROI) across hemispheres (Table 1). These ROIs were naturally divided into two spatially discontiguous clusters that covered PCC and mPFC, thus facilitating the study of each general region separately.

Meta-analysis

We used a novel approach to cortical surface parcel-based meta-analysis to assess whether individual parcels were differentially associated with valuation or DMN effects. For subjective value, we gathered peak brain coordinates of activity from 198 studies that were associated with positive effects for current or prospective rewards (Bartra, McGuire, and Kable 2013). For DMN, we acquired coordinates from a previous meta-analysis of 80 studies that were related to task-deactivation (Laird et al. 2009). These coordinates represent the surviving areas post-statistical thresholding from each study. For each study, we created an indicator map in standard space (MNI152, 1 mm resolution) which contained values of 1 in a 10 mm radius sphere around each reported activation peak, and values of 0 elsewhere (Wager et al. 2009). The indicator map for each study was then projected to a standard cortical mesh (fs_average, 32,000 vertices, projfrac-max from 0 to 1 by 0.25) using FreeSurfer's mri_vol2surf (Fischl 2012) (<http://surfer.nmr.mgh.harvard.edu/>). Any sphere

sections that overlapped with the cortex were mapped to our ROIs, and we tallied how many studies had positive indicator values in each parcel.

With these lists, we identified areas that were significantly more associated to either literature. We permuted the label of every study (i.e. DMN or valuation) 5000 times while preserving the total number of studies observed in each domain, and on each iteration stored the maximum resulting statistic (across all parcels) from chi-squared tests of proportions that compared the number of studies that contained each area. This gave us a null distribution of 5000 chi-squared values. The 95th percentile of this distribution served as an FWE-corrected significance threshold to evaluate unpermuted chi-squared values.

fMRI Data

Our fMRI analyses used resting-state fMRI data from the Human Connectome Project (Van Essen et al. 2012) Q6 release ($n = 100$, randomly sampled from the total pool of 469 available subjects). Each subject's data was acquired over two days at Washington University in St. Louis on a Siemens CONNECTOM Skyra MRI scanner (Siemens, Erlangen, Germany). Four resting state runs ($TR = 0.720$ s, $TE = 33.1$ ms, $FA = 52^\circ$, multiband factor = 8, 72 slices, 2 mm isotropic voxels) each comprised 1200 time points(14 min 33 s) for a total of 4800 time points. Two runs were acquired on each day, with the phase encoding direction set to left-right for one run and right-left for the other. Only subjects with both left-right and right-left phase encoding were included (i.e. subjects with four rsfMRI sessions). In addition, only datasets with either low motion levels (under 1.5mm) or under 0.5 mm mean framewise displacement (FD) were used.

Data initially underwent the HCP minimally preprocessing pipeline (M. F. Glasser et al. 2013), which included considerable gradient nonlinearity correction, motion correction, EPI distortion correction, temporal denoising based on independent components (FIX, (Griffanti et al. 2014; Salimi-Khorshidi et al. 2014)), high-pass filtering (0.0005 Hz threshold), and MNI152-based normalization. Data were further preprocessed using an in-house pipeline described previously (Tobeyne et al. 2017). Steps included linear interpolation across timepoints with over 0.5 mm of framewise displacement, band-pass filtering (allowed frequencies ranged from 0.009 and 0.08 Hz), temporal denoising and high-motion censoring by deletion, as well as mean greyordinate signal regression (Burgess et al. 2016). Volumes that displayed an FD of over 0.5 mm were considered as spikes and removed from the subject's dataset, and subjects whose spike counts were above 5% of their total data were excluded from analyses. Finally, data acquired on the same day (i.e. left-right and right-left phase encoding session) were temporally demeaned. Each subject's brain was comprised of 32k standard HCP greyordinates per hemisphere (combined in a CIFTI file). We retained only the cortical

surfaces, which resulted in 59,412 total surface vertices per subject.

Within-ROI Network Definition

All network analyses were performed using the igraph package (G. and T. 2006) in R 3.4.1 (R Development Core Team 2018). To establish each subject's network, we selected all the vertices contained within the ROIs ($n = 4,801$ per subject) and computed the Pearson correlation of the time series for every pair of vertices. This produced a weighted network for each subject, where surface vertices were the nodes, and edges the correlations among all of them. Next, we applied Fisher's r to z transformation, and performed a two-sided significance test to identify strong correlations. The resulting p-values were corrected for multiple comparisons (FDR < 0.05), and edges with non-significant correlations were turned to 0 (all other edges retained their respective z-values). Next, we took the exponential of these values so that all weights were positive while maintaining the ordinal ranks of the original correlation distribution. Values of 1 of this transformed distribution were returned to 0 in order to avoid the inclusion of these edges in the network analyses. We report the proportion of retained edges (i.e. network density) in the Results section. As part of the evaluation step, we produced these network weight matrices (and the community detection outlined below) at four levels: 1) for each run separately (1200 TRs each); 2) for the concatenated time series for the two runs on the same day (2400 TRs total); 3) for each subject's full dataset (4800 TRs total); and 4) on each step of a sliding window analysis (see Partition Evaluation for more details).

Community Detection

Communities (i.e. clusters) were identified by means of spectral partitioning (Fiedler 1975; Belkin and Niyogi 2003). First, each network was represented as an $n \times n$ network weight matrix (where $n =$ number of vertices within the ROIs, 4,801). This matrix was then transformed into its normalized Laplacian form

$$L = I - D^{-\frac{1}{2}}WD^{-\frac{1}{2}}$$

Where I is the identity matrix, D is a diagonal matrix containing the strength of each vertex (i.e. the sum of its correlation values with every other vertex), and W is the network weight matrix. This resulted in a matrix wherein each entry was the normalized value of the connection (from 0 to 1) between any two vertices relative to their combined connectivity strength, and with ones along the diagonal. This transformation ensures that every row adds up to zero. We then computed the eigenvalues and eigenvectors of the normalized Laplacian,

and used the eigenvector associated with the second-to-lowest eigenvalue to divide the network into two. This vector (traditionally called the ‘Fiedler vector’) provides a set of positive and negative values to binarize the network with (Fiedler 1975). This method enforces the partition of a network into similarly-sized communities, and guarantees that they share at least one edge (Chung 1999). In this way, spectral partitioning avoids producing communities that are too small to be physiologically meaningful (for example, small sets of vertices that are spuriously correlated due to measurement noise). Every individual partition is therefore binarized by sign in order to evaluate the topography of each community (see next section for details). Given that this data-driven method does not label the two communities or establish correspondence across participants, we defined each individual’s “DMN” community to be the one containing the DMN-specific PCC parcel identified in our meta-analysis. The high density of these networks (see Results) ensured that spectral partitioning did not face the issues associated with its use in sparse networks (Fortunato and Hric 2016).

In order to evaluate the convergent validity of the resulting partitions across community-detection methods, we also estimated these communities using the more traditional approach of modularity maximization, based on the algorithm from Clauset et al. (2004). *(TBD) This method maximizes a quality function that compares the strength of the connection between any two vertices against a null model of their probability of being randomly connected to any other vertex in the network. The method heuristically iterates through many possible combinations of vertices, and selects the clustering that maximizes the network’s modularity.* Unlike SP, modularity can fractionate a network into more than two functional groups. We assumed that if the partitions from the bounded and unbounded community detection methods showed high levels of agreement, we could gain confidence in that we are indeed fractioning the ROIs into those belonging to DMN and not. We also diagnosed our choice of two communities by reporting the rank (from lowest to largest) of the first eigenvalue produced by spectral partitioning to be non-zero. This eigenvalue serves as an estimator of the optimal number of communities in a network (Chung 1999), such that a rank of two in our partitions justifies limiting the number of communities to two.

Partition Evaluation

In order to evaluate the stability and topographical heterogeneity of the communities within and across subjects, we chose the adjusted rand index (ARI) as the reference metric of agreement between two clusterings (Hubert and Arabie 1985). The base of the ARI is computed by the formula

$$\frac{a + b}{a + b + c + d}$$

Where a is the number of pairs of nodes that were grouped together in both partitions, b is the number that were grouped separately, and c and d denote the number grouped together (separately) in one partition, but separately (together) in the other. Therefore, ARI estimates the ratio at which every pair of nodes in partition A were jointly assigned to the same/different parcels on partition B, over all possible relational changes. The resulting ratio is adjusted by comparing it to a baseline given by the expectation of a random node assignment across partitions. This means that even though clustering deviations are heavily penalized, positive ARI values compare favorably against chance clustering (and can take negative values if the index given by the formula above falls below 50%). In short, the ARI determines the chance-corrected percentage of agreement between any two partitions while being agnostic to the labeling scheme.

We performed a number of comparisons among partitions. First, we computed the degree of agreement between SP and modularity per subject to validate the resulting functional patterns. Modularity and SP have been previously found to show overfitting and underfitting tendencies, respectively, in their community detection performance in a diverse number of network types (Ghasemian, HosseiniMardi, and Clauset 2018). Their alignment would thus give us confidence in the validity of the resulting topologies. Next, we compared the functional organization derived from the whole time series across subjects, and report the mean pairwise ARI for the group. We then performed the same evaluation for PCC and mPFC separately, and examined whether there are mean differences in overall agreement within these regions by performing a paired permutation analysis (5000 iterations) on all pairwise ARI comparisons across subjects. Given that the functional heterogeneity of brain areas is unevenly distributed across the cortex (Mueller et al. 2013), we performed all the subsequent analyses on PCC and mPFC separately.

To estimate the degree of stability of these partitions per subject we performed a sliding window analysis (20 min windows, 1 min increments, mean number of windows per subject = 37), comparing each window's resulting partition against the partition derived from the whole subject's data. A 20-min window is typically adequate for identifying stable community features in brain networks (Gordon et al. 2017). We assessed whether the magnitude of the Fiedler vector value for a given vertex (for the full subject-level data set) was associated with the stability of that vertex's sub-network assignment across time windows. To do this, we fit a mixed effects logistic regression model, in which the dependent variable was the proportion of times each vertex participated in the DMN community across windows, and the explanatory variables included a random effect of subject and a fixed effect of the Fiedler vector value for that vertex (derived from their full time series). Based on this relationship, we identified a threshold of Fiedler vector values for each subject, such that vertices above these thresholds were persistently associated with either DMN or non-DMN over 95% of the time.

We then estimated the level of agreement between network partitions estimated using data from individual days (with 2 days per participant). If the functional organization estimated by SP is indeed subject-specific, we should see higher agreement within subject (test/re-test across days) than across subjects. We tested this idea by computing the ratio of the mean ARI within and between subjects. Ratios close to one denoted similar within-subject and across-subject alignment, whereas ratios considerably higher than one suggested that partitions were more similar within-subject than across subjects. We then extended this idea by computing the overall agreement across all runs (4 per subject) Similar to the day-based analysis, we assessed whether session-level data showed higher agreement within-subject than between subjects.

Seed-based FC vs Community Detection

We evaluated the performance of the spectral partitioning algorithm in comparison to a simpler partitioning approach using seed-based functional connectivity. First, we estimated each subject's DMN partition in mPFC based on its vertex-wise functional correlation (Pearson) with the average PCC activity for each day separately. We compared these seed-based maps with the Fiedler vectors produced by SP by spatially correlating them across days and subjects in three ways: 1) between seed-based maps; 2) between SP-based maps; and 3) between seed- and SP-based maps. These spatial correlations were aimed to determine the test/re-test reliability of each approach, as well as the overall level of agreement between them. The two methods were expected to produce somewhat similar arrangements, but the one displaying the higher within-subject agreement across days should be preferred (for a discussion on the stability of functional networks see (Kong et al. 2018; Mueller et al. 2013)). We thus compared the mean within-subject inter-day correlation coefficients of each method through a paired permutation analysis (5000 iterations).

Results

Meta-analysis

We performed a coordinate-based meta-analysis to identify unique standard regions across DMN and SV literatures. Volumetric coordinates from a set of DMN and SV studies were projected onto a cortical surface, and mapped to a multimodal cortical parcellation (M. F. Glasser et al. 2016) to produce a list of brain areas reported per study. The 45 areas considered were limited to the medial portion of the default mode and limbic networks, as defined by the Yeo et al.'s (2011) 17 network parcellation. Unique areas were identified by first permuting the affiliation of each study (i.e. DMN or SV) to create a distribution of chi-squared statistics

based on the comparison of the number of reports per area between literatures (see Methods for details). This putative null distribution was used to identify regions more often reported in either literature.

Figure 1 shows the proportion of times every parcel was reported in each literature, as well as the resulting significant ROIs from the permutation. The 95th percentile of the permuted chi-squared distribution was 9.11. Based on this threshold, area 7m was the only one to show unique bilateral affiliation to DMN (Left: observed $\chi^2 = 10.07, p = 0.034$; Right: observed $\chi^2 = 18.89, p < 0.0001$), while SV was uniquely represented bilaterally by area 25 (Left: observed $\chi^2 = 12.91, p = 0.014$; Right: observed $\chi^2 = 12.83, p = 0.014$). The purpose of these supra-threshold areas was to identify the most-likely affiliation of the two communities in our partitions by their coverage of these regions. However, area 25 sits in close proximity to the ventral striatum, which is reliably active in SV studies (Bartra, McGuire, and Kable 2013). Considering that our projection from volumetric spheres to the cortex might have attributed striatal reports to this region, we decided not to use it as a marker of SV. We also chose not to use area v23 due to its unilateral significance (Right: observed $\chi^2 = 11.51, p = 0.018$). Instead, we only rely on area 7m to demarcate the DMN community.

Partition Comparison: Full Datasets

With these 40 ROIs (38 overlapping, 1 DMN-specific, and 1 SV-specific), we estimated each individual's DMN coverage using their full time series (approximately 4800 total TRs from four scanning sessions over two days). Each subject's network ($n = 100$) was constructed by performing pairwise correlations among the time series of all the surface vertices contained within the ROIs (4801 total vertices). After correcting for multiple comparisons, we performed spectral partitioning on these networks to identify cohesive functional communities denoting DMN and non-DMN areas. On average, networks had high densities (i.e. highly connected) regardless of whether they were produced with a single run all the full time series (mean = 0.95, SD = 0.011). This high degree of density is important, as this method is known to face challenges when computed on sparse networks (Fortunato and Hric 2016).

Figure 2 shows a stereotypical subdivision of the ROIs for a single subject (100307) using spectral partitioning. This method dissects a network by the positive and negative values derived from the Fiedler vector (the eigenvector related to the second-to-lowest eigenvalue of the network's Laplacian matrix, see Methods), which we used to binarize the ROIs. Since this is a data-driven approach, there is no a priori labeling for these communities. We thus defined the DMN community as the one containing the one DMN-specific area from the meta-analysis (7m), and ensured that the binary labeling of the vertices was consistent across subjects. In general, the resulting pattern shows large DMN coverage in PCC, with non-DMN vertices populating its

anterior segment. On the other hand, mPFC is mostly covered by DMN vertices in its ventral-anterior and dorsal-anterior areas, with a persistent non-DMN pocket between them. This non-DMN section extends posteriorly onto pregenual cingulate cortex (area a24).

Before determining the degree of generalizability of this topological pattern across individuals, we examined the validity of these partitions by comparing them to patterns derived with a modularity algorithm (Clauset, Newman, and Moore 2004). Modularity seeks to find the pattern of communities that maximizes a quality function that compares the connectivity strength of any two nodes with a null probability model. Since modularity is not bound to a desired number of communities, it was capable of finding more than two in our dataset. We quantified the cross-method agreement with the adjusted rand index (ARI). ARI measures the proportion of pairs of nodes in a network that were either clustered together or separately in both partitions, over all possible affiliation changes. This measure has the benefit of being agnostic to labeling schemes, as well as controlling for the expectation that the clusters were randomly produced (Hubert and Arabie 1985). This means that positive ARI values compare favorably against chance clustering.

This comparison showed that both clustering methods were in high agreement across subjects (mean = 0.87, SD = 0.11). Modularity showed a tendency to produce additional communities (median = 3, max = 4). However, these communities encompassed a small number of vertices (mean = 32.0375, IQR = 33.625) compared to the principal two (mean = 2387.155, IQR = 13.875), suggesting that the overall network is composed of two main communities. In addition, the estimation of the optimal number of cuts based on the rank of the first non-zero eigenvalue (see “Partition evaluation” for details) showed that 100 percent of the individual networks are best partitioned into two communities.

Next, we examined how similar the partitions were across subjects by computing the ARI between every pair of subjects, and found that there was moderate agreement overall (mean = 0.12, SD = 0.05). However, qualitative inspection of the brain community topologies showed good alignment for PCC, with a topologically similar mPFC pattern that shifted topographically across subjects. To quantify this heterogeneity in mPFC, we performed the same analysis for each region separately (Figure 3). Indeed, this analysis showed that the functional topology of PCC is better maintained across subjects (mean = 0.18, SD = 0.09) than mPFC (mean = 0.09, SD = 0.04) (paired permutation, $p = 0$; Cohen’s D = 1.34).

Pattern stability over time

In order to estimate the degree of stability of these partitions in time, we performed a sliding window analysis on each subject’s full time series (20 min windows shifting at 1 min), comparing the community arrangement

derived from each window with the partition computed using the whole time series (Figure 4).

This analysis showed that the mean ARI along each subject's time series was high for both PCC (mean = 0.59; SD = 0.14) and mPFC (mean = 0.49; SD = 0.12), with significantly higher ARI for PCC (paired permutation, $p = 0$; Cohen's D = 0.71). These results suggest that the each individual's DMN distribution is considerably stable in time.

There is precedence in the literature that the magnitude (and not just the sign) of the Fiedler vector values conveys important information about the role of each node in the network (Gkantsidis, Mihail, and Zegura 2003; Tian and Zalesky 2018). Therefore, we asked whether the magnitude of these eigenvector values was associated with the stability of nodes in time. Specifically, we examined whether Fiedler vector values could predict the proportion of DMN affiliations per node by performing a logistic mixed effects model (Figure 5). The model yielded a positive significant relationship between these features ($\beta = 211.54$, SE = 0.51, $p < 0.001$), meaning that vertices with higher absolute Fiedler vector values were more persistent in their relationship with their corresponding community in time. We refer to this proportion of affiliations over time as the stability of a given node.

These analyses show that the original pattern identified with the full dataset is stable in time, and that there is potential value in thresholding the Fiedler vector as a means to capture idiosyncratic and reliable DMN and non-DMN vertices, even in relatively short resting fMRI sessions (i.e. less than 20 mins). We therefore thresholded each subject's Fiedler vector to produce these refined maps. We estimated this threshold by selecting the smallest absolute Fiedler vector value that yielded a stability of 95%, for positive (mean = 0.0132, SD = 0.0051) and negative (mean = -0.0144, SD = 0.0056) values separately. Individuals without such stable nodes ($n = 17$) were not thresholded, but their partitions were not discarded. Vertices under these thresholds were set to zero (instead of removed) so that the dimensionality of the data was unaffected, and 0.5 in the binarized maps so that they wouldn't bias the calculation of averages. Figure 6 (left) shows the updated partition for the one showed in figure 2. The maps used in all subsequent analyses were thresholded by this individualized criterion.

Partition Comparison: Thresholded Full Datasets

The average percentage of stable vertices per subject was 0.41 (SD = 0.18). With these thresholded partitions, we recomputed the overall similarity of their functional organization across participants. Compared to before, there was even less overall agreement of the full maps among individuals (mean = 0.07, SD = 0.04). The same was true for both PCC (mean = 0.11, SD = 0.07) and mPFC (mean = 0.04, SD = 0.03) separately, although

the significance of the differences between these areas was preserved (paired permutation, $p = 0$; Cohen's D = 1.2). Figure 6 (right) shows the spatial average of the thresholded binarized partitions across all participants, denoting the proportion of times a vertex was affiliated with the DMN community. This summary conveys a common organizational principle for both communities, but also highlights the considerable variability across individuals in mPFC compared to PCC.

To discard the possibility that the higher inter-subject variability in mPFC was driven by retaining vertices with lower signal quality, we compared the mean temporal signal to noise ratio (tSNR) for each region pre and post thresholding. We used subject time series that were not demeaned, but were otherwise equivalent to the data originally used. Paired permutation analyses (5000 iterations) showed that the mean tSNR in mPFC actually significantly increased post-thresholding across subjects (Pre: mean = 66.5011992, SD = 7.8670576; Post: mean = 77.7216815, SD = 14.5412332; paired permutation p-value = 0, Cohen's D = 0.9597906), whereas the mean signal quality in PCC was unaffected (Pre: mean = 64.5575973, SD = 10.0241371; Post: mean = 64.7835568, SD = 10.3244531; paired permutation p-value = 0.2528, Cohen's D = 0.0222064).

Partition Comparison: Day 1 vs Day 2

The relative high variability seen in the aggregate map could be due to variations in the functional organization of mPFC across days. While the sliding window analysis suggested that these partitions are stable, many of the windows contained data from both days. A stricter evaluation of subject-specificity would be to compare every subject's subdivisions produced by data from each day separately. If the variability that we observed was truly due to having captured an individual's unique organization, day to day ARI values should be consistently higher within- than between-subjects. Figure 7 shows pairwise comparisons among ten example subjects for whole brain (left), as well as for PCC and mPFC separately (right).

Once again we found low alignment across subjects for PCC (mean = 0.08, SD = 0.06) and mPFC (mean = 0.04, SD = 0.03), but both areas showed relatively high levels of agreement within subjects (PCC: mean = 0.36, SD = 0.14; mPFC: mean = 0.26, SD = 0.1). However, a coarse comparison of mean ARIs neglects the degree to which subject-wise partitions were indeed idiosyncratic. Therefore, we divided everyone's within-subject ARI by the mean ARI of their between-subject comparison. This ratio denotes the relative specificity of their partition, such that partitions that align well across subjects should yield ratios close to 1, while unique and stable partitions would produce high ratios. Given what we know about these general regions, we expected PCC to be well aligned both within and between subjects. On the other hand, we hypothesized low agreement of mPFC partitions across participants, but with considerable stability across

days and sessions within subject.

Figure 8 shows these ARI ratios for PCC and mPFC for all subjects. As expected, we found that while both regions had good specificity (i.e. ratios > 1), the ratios for mPFC (median = 7.38; SD = 3.74) were significantly higher than those for PCC (median = 4.3; SD = 8.04) when compared with a paired permutation test ($p = 0$; Cohen's D = 0.33). These test/retest results suggest that the topographic variability seen in mPFC is reliably rooted in subject-specific organization, and not an inability to capture its topology.

Partition Comparison: Session based

We extended the analysis of daily data by examining whether the organization of the DMN could be extracted using session data only. It is worth noting that the length of each session (approx. 14 mins long) falls below the stability threshold for fMRI-based modularity estimations (Gordon et al. 2017). Nonetheless, high ARI ratios with reduced data could signify the ability to localize a subject's DMN organization with fMRI sessions that are easier to fit along with other study sessions of interest.

Computing SP on networks from individual sessions showed that we can still coarsely capture a subject's unique organizational pattern (Figure 9), even though the overall levels of agreement decreased (PCC between subjects: mean = 0.04, SD = 0.05; PCC within subjects: mean = 0.17, SD = 0.14; mPFC between subjects: mean = 0.02, SD = 0.02; mPFC within subjects: mean = 0.1, SD = 0.08). We again computed each subject's ARI ratio in order to quantify the specificity of these partitions, but this time using the mean ARI across sessions (Figure 10).

We can see again that the ratios for mPFC were higher than those of PCC (permutation, $p = 0$; Cohen's D = 1.1), but both were mostly above 1. This further confirms that the intrinsic functional organization of mPFC is uniquely arranged per individual, and provides evidence that such patterns can be identified with small amounts of data in spite of a reduction in the estimates.

Correlation vs community detection in mPFC

The computational demands of our approach escalate quickly as the number of vertices increases. We thus explored the possible advantage to using community detection over a simple seed-based functional connectivity analysis from PCC. Given that other groups have found the spatial distribution of the DMN to be considerably stable within individuals (T. O. Laumann et al. 2015; Gordon et al. 2017; Braga and Buckner 2017; Kong et al. 2018), we examined whether maps generated with spectral partitioning were more similar per subject

across days than those computed from seed-based correlations. First, we computed each individual's mean time series of all the vertices contained within PCC, and correlated it with the activity of every mPFC. Since correlation values are continuous, we compared them to their respective unbinarized Fiedler vector maps. We performed pairwise spatial Pearson correlations among maps computed for each day and method from all subjects. For 3 subjects, the maps produced with one of the days' datasets insufficiently covered area 7m, and so the community labeling was reversed (for one additional subject, both daily maps were reverted). ARI is robust to these labeling issues, but this produced strong negative correlations of the Fiedler vector for these subjects, even though the topography was highly similar. We thus visually inspected these subjects ($n = 7$) and reverted the labeling when it was clear that the topologies aligned across days. Figure 11 shows that these pairwise comparisons resemble those from the day-to-day comparisons above, and suggests good alignment between methods, but particularly high agreement within subject and method.

Figure 12 shows the overall degree of similarity across days for patterns derived using community detection, seed-based correlation, and across methods (i.e. day one community detection versus day two seed-based correlation). While both approaches are very consistent, community detection displayed a significantly higher ARI across days than a simple correlation (paired permutation $p < 0.001$; Cohen's D = 0.45). It is worth noting that the cross-method agreement is fair, meaning that both approaches show similar topological features. These findings suggest that graph-theoretic community detection algorithms provide a better way to detect stable functional topologies.

Similarities with other work

The thresholded partitions in our work qualitatively resembled the topographical arrangement of networks A and B proposed by Braga and Buckner (2017). We explored this similarity by reproducing their seed-based connectivity approach in three of our subjects. In their work, Braga and Buckner selected individual vertices along the dorsolateral prefrontal cortex (DLPFC) that produced these two anticorrelated networks. Therefore, we hypothesized that if the communities we identified on the medial wall matched their proposed networks, we should be able to find seed vertices in DLPFC that can reproduce them. The whole-brain seed-based functional connectivity maps for these subjects are juxtaposed to their spectral partitioning counterparts on figure 13.

Visual inspection of these networks shows a remarkable similarity between our DMN and non-DMN communities and their networks A and B. These qualitative results are important, as here we reinforce the idea that canonical DMN can be reliably subdivide at the individual level. Further, it shows the potential of

community detection methods to automatically extract these partitions without the need to rely on group data. One way in which our results are at odds with those from Braga and Buckner is the functional labeling of these sub-networks. Based on our criteria, network B would more closely identify with DMN (per 7m affiliation), while we currently do not have enough evidence to label network A. These discrepancies should be addressed with explicit behavioral manipulations in the future.

Discussion

For clinical implications, see Hiser & Koenigs 2018. In short, being able to identify functional idiosyncrasies without much data can yield important insights in diagnosis (meh, we always say that..) of a variety of psychological diseases associated with mPFC. It would be more interesting to identify the repercussions of damage in mPFC per individual. They mention that subgenual vmPFC is a common target for deep brain stimulation (or TMS) as a depression treatment. The refinement of the technique is thus coupled to being able to identify personalized functional topologies. They list a number of results related to mPFC functional connectivity too. In the end, their suggestions for clinical implications of mPFC studies rely on the individual measure of functional expanse. (note that social-relevant areas in their meta analysis look similar to our patterns, and the emotion part to Barbas' latest)

It will also be good to note that there is concurrent debate on the ground truth of community detection. In other fields, identifying a community structure is not necessarily associated with the true organization of the network. What happens is that you might find a tangential grouping that gives you information different from your original goal (Clauset, Newman, and Moore 2004). In our case, however, averaging everyone's partitions produces organizational maps that resemble those from previous work (e.g. Margulies).

Talk about how there are other community detection algorithms, and that modularity and SP over and underfit, respectively. However, SP eigenmaps have been found to provide relevant functional information. In addition, both modularity and SP rely on connectivity strength, and thus is amenable to the correlative nature of functional connectivity.

Interhemispheric differences? citing Mackey and Petrides

And write a portion on the lack of subcortical reward-related regions (i.e. striatum). Say something like ‘incorporating the ventral striatum did not refine these partitions through either method. This could be due to the lack of signal modulation of this area at rest, and should be examined through behavioral manipulations of value in the future. Instead, here we focus on capturing the intrinsic functional heterogeneity of mPFC as a way to pave the path to refined analyses aimed at disentangling DMN and SV’. It is worth noting that the

SV-only area from the meta-analysis tends to land in non-DMN, although it ends up in no-ones land when thresholding the maps.

It might also be worth mentioning that previous work has established the shift in network types during rest through hidden Markov models (Vidaurre et al., 2016?). While this suggests that we should see fluctuations in affiliation, and not stability, Vidaurre's work establishes the dynamics of prevalent function among networks, and not their topologies. Our work focuses on the topographical arrangement of the DMN network, which can be active or not while maintaining its form. So, the two works are compatible. Note, I played a bit with AR and MA processes per subject to try to understand the autocorrelation in the sliding window. First, both `acf/pacf` and `arima (order = n,0,n)` R functions suggested that the data was better fit by AR. Moreover, ARs from 1 to 10 had negligible differences, so I stuck with 1 results for simplicity. As expected the data is significantly autocorrelated, and when I checked plotted the residuals they were mostly within the 0.15 bound (normally distributed). Coefficients ranged from 0.6 to 1. So, there is clear rhythmicity in the agreement between each window and the overall pattern. However, the intercepts from the ARn processes gave more or less the same estimates as the mean rand index over all the windows. This is mostly expected, as we saw that the standard deviation of the rand index was low across participants. I am currently interpreting this as a signal that there is clear periodicity that is otherwise harmless for our results: in the end, the agreement remains stable throughout the 4800 TRs.

In terms of noise, there are a handful of things to keep in mind. First is that yes, mPFC is noisier overall, but that did not preclude the relatively high levels of agreement across days and sessions per subject, even though ARI heavily penalizes discrepancies (less than linearly). Second, low R^2 values were found all throughout the z-axis, meaning that variance explained is not strictly determined by the cardinal position of the vertex (and while the correlation was significant due to the sheer number of items, the coefficient was relatively low). Right now this might be ok as a way to bypass noise comments, but it would also be interesting to take advantage of the Fiedler vector here. Since it's linearly related to R^2 per subject, perhaps finding a way to threshold these values would provide cleaner and even more consistent maps.

So what's the advantage of this work over previous ones? Gratton, Gordon, and Kong have already found some degree of subject stability and intersubject variability. Ours complements these findings by looking at the vertex level, not just mean parcel activity (this made sense for them, as they were looking at the whole brain). Also, most of these analyses rely on a small set of oversampled subjects (i.e. MSC). Here we extend this to 100, giving credit to individualized examinations even without oversampling.

Make sure to emphasize that the high overlap between sliding windows makes it more likely that differences

are due to noise in the signal, and not strong variability. Like, you wouldn't expect the actual network distribution to shift that much after shifting the time series by 1 minute.

Acknowledgements

We would like to thank Dan Sussman for initial guidance on community detection and evaluation methods. Data were provided [in part] by the Human Connectome Project, WU-Minn Consortium (Principal Investigators: David Van Essen and Kamil Ugurbil; 1U54MH091657) funded by the 16 NIH Institutes and Centers that support the NIH Blueprint for Neuroscience Research; and by the McDonnell Center for Systems Neuroscience at Washington University.

Supplemental Materials

Table 1. Regions of interest from Glasser et al. (2016). Prefixes indicate hemispheric location (e.g. R = right).

Literature	Significant Brain Regions
ROIs	L_25, L_OFC, L_10v, R_25, R_OFC, R_10v, L_s32, L_RSC, R_RSC, R_23d, R_d23ab, R_31a, R_31pv, R_31pd, R_7m, R_v23ab, R_p24, R_d32, R_9m, R_p32, R_a24, R_10r, R_10d, L_23d, L_d23ab_RO, L_31a, L_31pv, L_31pd, L_7m, L_v23ab, L_p24, L_d32, L_9m, L_p32, L_a24, L_10r, L_10d, R_s32, R_9a, L_PCV

Figures

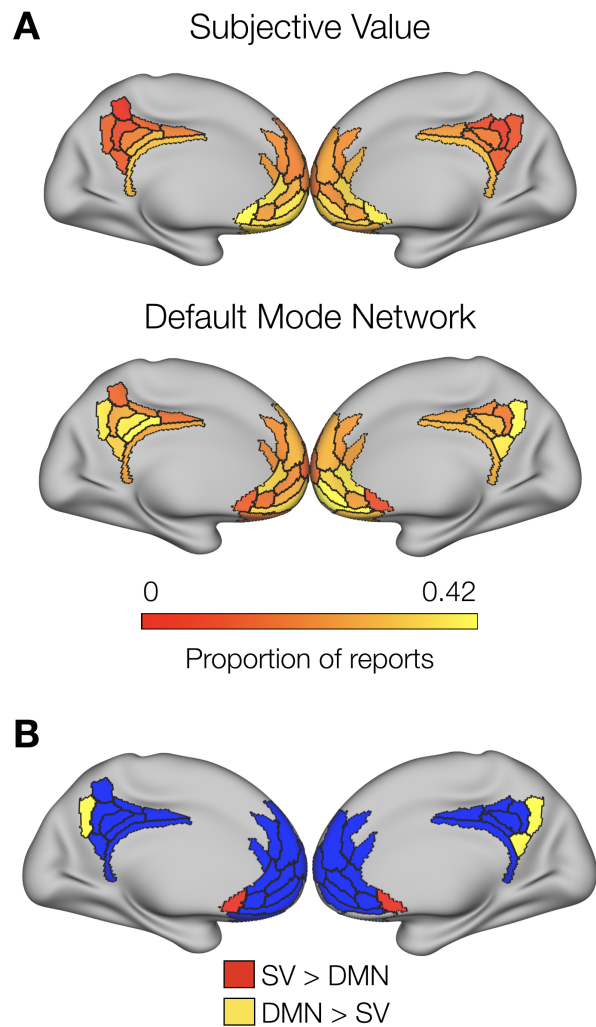


Figure 1: A: Proportion of times each ROI was reported in each literature. B: common and unique brain regions associated with DMN and subjective value. DMN regions defined by Yeo et al. (2011) in blue, which encompass areas of considerable overlap between DMN and SV. Literature-specific regions (bilateral 7m and right v23 in yellow, and bilateral 25 in red) were identified from a permutation analysis of chi-squared tests comparing these literatures.

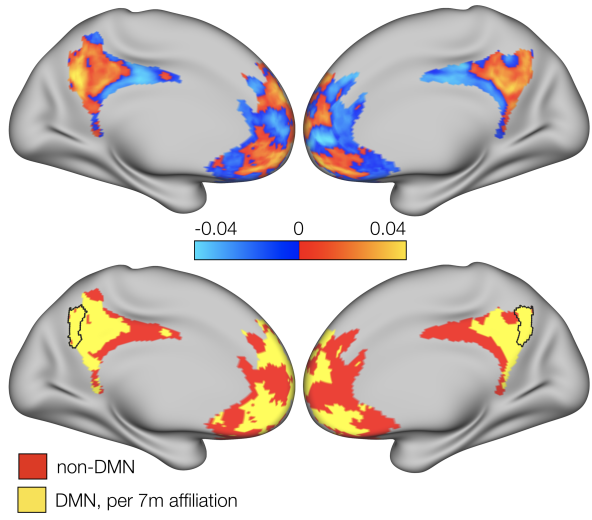


Figure 2: Brain partition for an example subject (100307). Fiedler vector values (top) are mapped onto the brain surface, dividing it into positive and negative communities. The bottom brain shows the binarized Fiedler vector, with yellow areas denoting the DMN community (as indicated by coverage of area 7m, bordered).

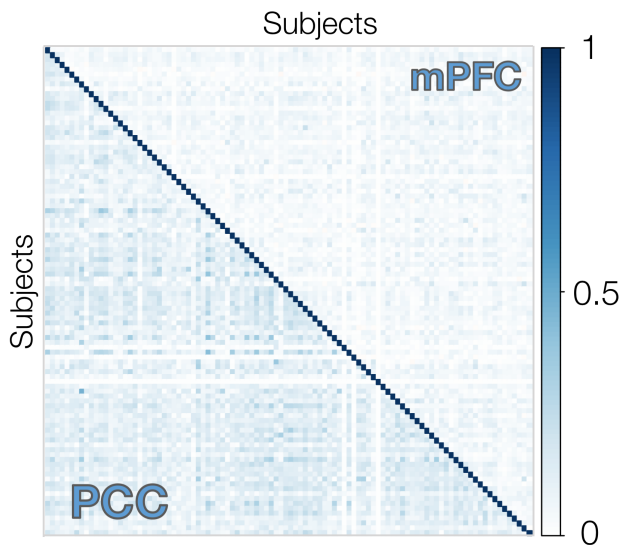


Figure 3: Similarity matrix showing ARI values among all subjects for PCC (lower triangle) and mPFC (upper triangle) separately. PCC is better aligned across individuals than mPFC.

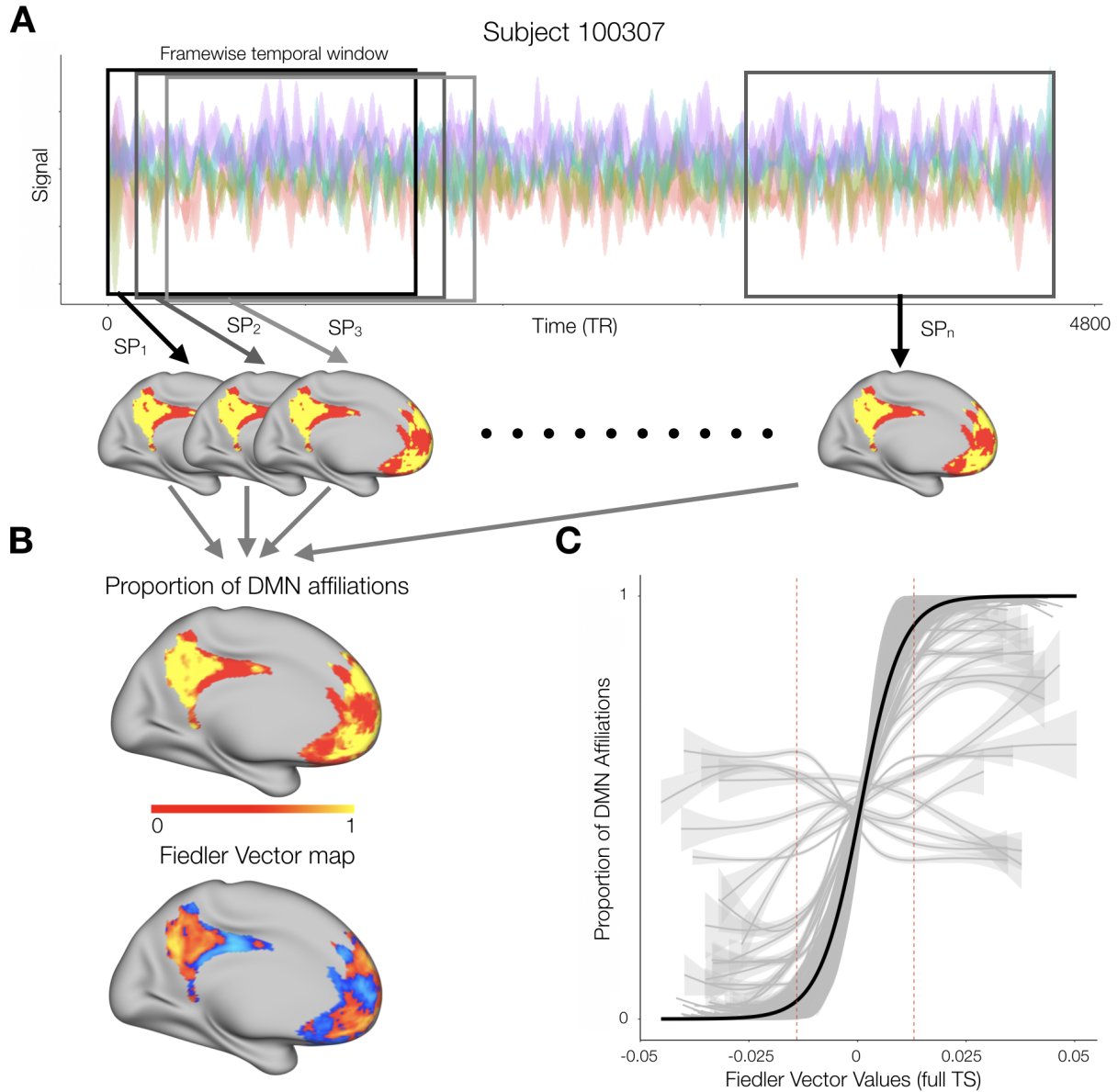


Figure 4: A: For each subject, we produced partitions for each 20 minute sliding window (1 min shift, 84 TRs) throughout their full time series (median number of windows = 37). B: Proportion of times each vertex was affiliated with the DMN community across windows (up), and the continuous Fiedler vector map for the current subject using their full time series (down). The maps share considerable qualitative similarities in their gradients along the cortical surface. C: Relationship between the magnitude of Fiedler vector values and the proportion of DMN affiliations. Grey lines display each subject's association, while the black line shows the fit from a mixed-effects logistic regression. Dashed red lines indicate the mean FV value at which maps were thresholded.

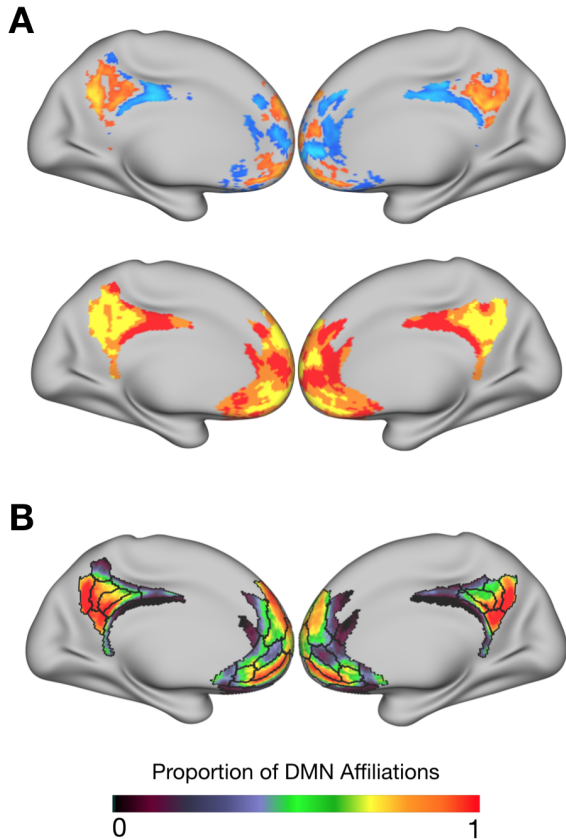


Figure 5: A: Thresholded Fiedler vector maps for subject 100307 (top), and its binarized form (bottom). Values that did not meet the threshold were set to zero on the Fiedler vector, and 0.5 on the binarized maps (giving rise to a third community of high-variability vertices). B: Spatial mean of the binarized maps across all participants, indicating the proportion of DMN affiliations per vertex in our sample. This aggregate map shows the common organizational principle of the DMN and non-DMN communities, while also pinpointing the relatively high level of variability in mPFC.

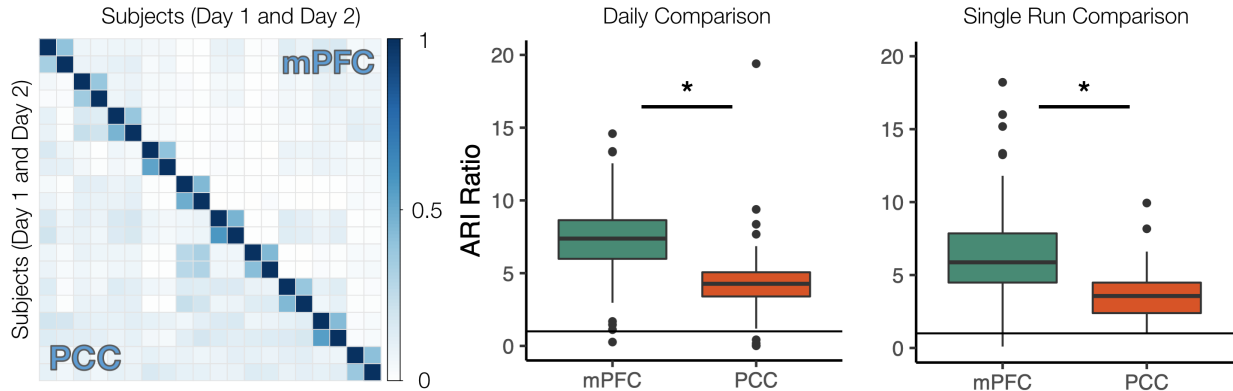


Figure 6: Left: Similarity matrix for 10 example participants (2 days of scans each), showing pattern agreement across days and subjects for PCC and mPFC separately. Middle: ratio of within-subject ARI to between-subject mean ARI for all individuals across days suggests idiosyncrasies in community arrangement for both PCC and mPFC (ratios > 1 , solid line), with higher subject-specificity in the latter. Right: within-to-between subject mean ARI ratios for each subject again show higher idiosyncratic organization for mPFC.

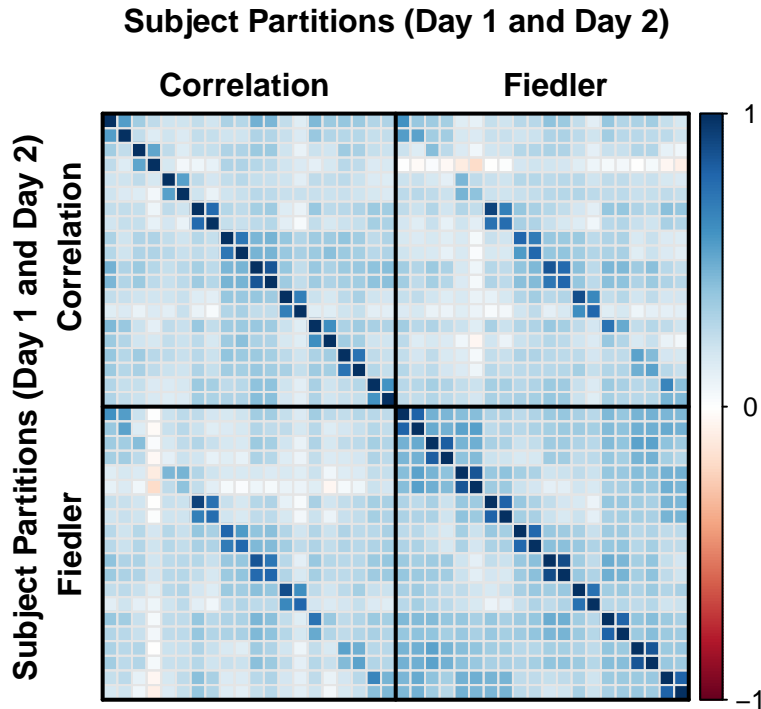


Figure 7: Correlation matrix comparing the inter-day spatial stability of maps derived from seed-based functional connectivity (PCC-based) and the Fiedler vector for 10 example subjects. The top-left quadrant represents seed-based FC maps, and the bottom-right the Fiedler vector. There is high agreement within method (diagonal quadrants), but both methods suggest similar partitions (off diagonal quadrants).

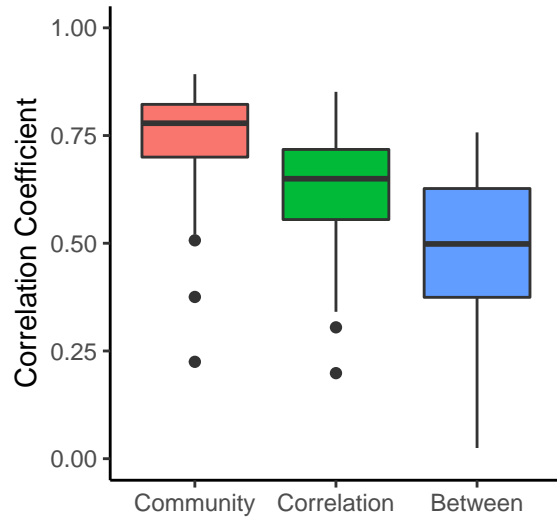


Figure 8: Day 1 vs Day 2 correlation coefficients for every method, as well as between methods. Community detection through spectral partitioning provides the most stable inter-day estimates, even though both methods show good level of agreement.

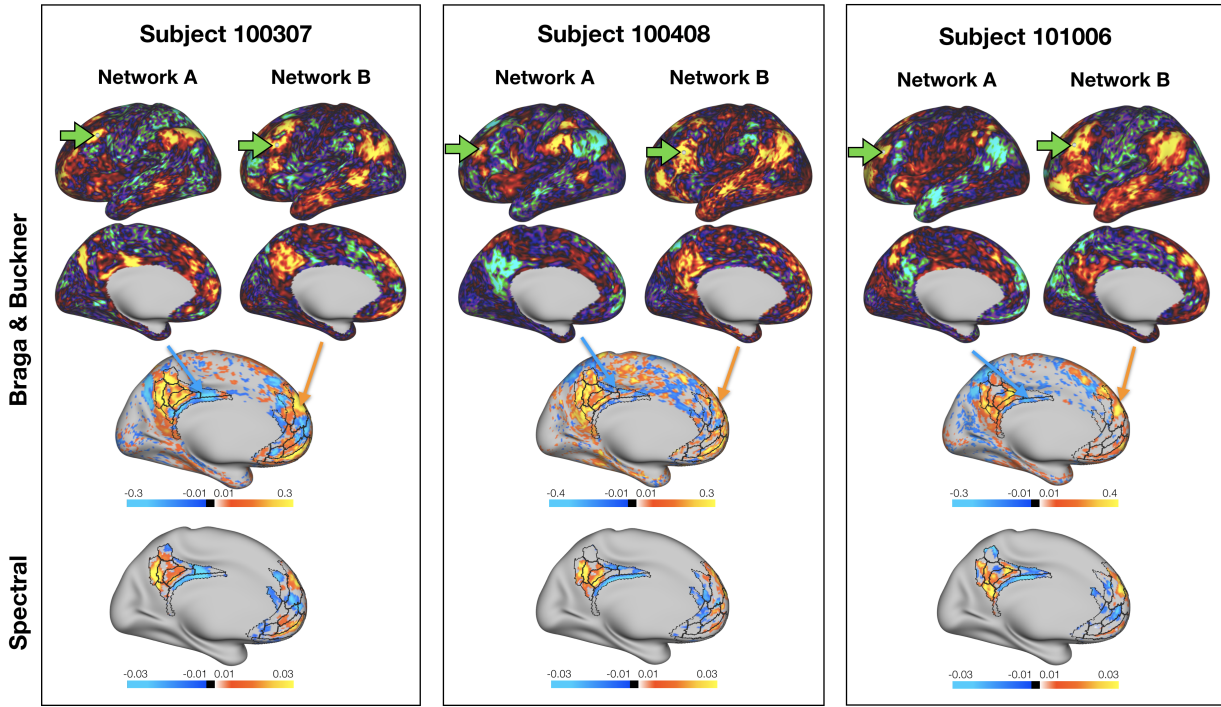


Figure 9: Qualitative comparison between maps produced by seed-based connectivity based on Braga and Buckner's (2017) criterion, and those produced by spectral partitioning. Networks A and B were produced by carefully selecting a DLPFC seed (pointed by the green arrows). In each case, our DMN and non-DMN networks map remarkably well to their proposed functional organization.

References

- Acikalin, M. Yavuz, Krzysztof J. Gorgolewski, and Russell A. Poldrack. 2017. “A coordinate-based meta-analysis of overlaps in regional specialization and functional connectivity across subjective value and default mode networks.” *Frontiers in Neuroscience* 11 (JAN): 1–11. doi:10.3389/fnins.2017.00001.
- Bartra, Oscar, Joseph T. McGuire, and Joseph W. Kable. 2013. “The valuation system: A coordinate-based meta-analysis of BOLD fMRI experiments examining neural correlates of subjective value.” *NeuroImage* 76. Elsevier Inc.: 412–27. doi:10.1016/j.neuroimage.2013.02.063.
- Bassett, Danielle S, Perry Zurn, and Joshua I Gold. 2018. “On the nature and use of models in network neuroscience.” *Nature Reviews Neuroscience*. Springer US, 1–13. doi:10.1038/s41583-018-0038-8.
- Belkin, Mikhail, and Partha Niyogi. 2003. “Laplacian eigenmaps for dimensionality reduction and data representation” 1396: 1373–96.
- Braga, Rodrigo M., and Randy L. Buckner. 2017. “Parallel Interdigitated Distributed Networks within the Individual Estimated by Intrinsic Functional Connectivity.” *Neuron* 95 (2). Elsevier Inc.: 457–471.e5. doi:10.1016/j.neuron.2017.06.038.
- Burgess, G. C., S. Kandala, D. Nolan, T. O. Laumann, J. D. Power, B. Adeyemo, M.P. Harms, S.E. Petersen, and D. M. & Barch. 2016. “Evaluation of Denoising Strategies to Address Motion-Correlated Artifacts in Resting-State Functional Magnetic Resonance Imaging Data from the Human Connectome Project.” *Brain Connectivity* 6 (9): 669–80.
- Chung, Fan R. K. 1999. “Review of Spectral Graph Theory.” *ACM SIGACT News* 30 (2): 14. doi:10.1145/568547.568553.
- Clauset, Aaron, M. E. J. Newman, and Cristopher Moore. 2004. “Finding community structure in very large networks” 066111: 1–6. doi:10.1103/PhysRevE.70.066111.
- Clithero, John A., and Antonio Rangel. 2014. “Informatic parcellation of the network involved in the computation of subjective value.” *Social Cognitive and Affective Neuroscience* 9 (9): 1289–1302. doi:10.1093/scan/nst106.
- Fiedler, Miroslav. 1975. “A Property of Eigenvectors of Nonnegative Symmetric Matrices and its Application to Graph Theory.” *Czechoslovak Mathematical Journal* 25 (100): 619–33.
- Fischl, Bruce. 2012. “FreeSurfer.” *NeuroImage* 62 (2): 774–81. doi:10.1016/j.neuroimage.2012.01.021.
- Fortunato, Santo, and Darko Hric. 2016. “Community detection in networks: A user guide.” *Physics Reports*

659. Elsevier B.V.: 1–44. doi:10.1016/j.physrep.2016.09.002.
- Fox, M. D., A. Z. Snyder, J. L. Vincent, M. Corbetta, D. C. Van Essen, and M. E. Raichle. 2005. “From The Cover: The human brain is intrinsically organized into dynamic, anticorrelated functional networks.” *Proceedings of the National Academy of Sciences* 102 (27): 9673–8. doi:10.1073/pnas.0504136102.
- G., Csardi, and Nepusz T. 2006. “The igraph software package for complex network research.” *InterJournal Complex Systems* 1695.
- Garcia, Javier O., Arian Ashourvan, Sarah Muldoon, Jean M. Vettel, and Danielle S. Bassett. 2017. “Applications of community detection techniques to brain graphs: Algorithmic considerations and implications for neural function.” *bioRxiv*, 209429. doi:10.1101/209429.
- Ghasemian, Amir, Homa HosseiniMardi, and Aaron Clauset. 2018. “Evaluating Overfit and Underfit in Models of Network Community Structure,” 1–17. doi:arXiv:1802.10582v2.
- Gkantsidis, C., M. Mihail, and E. Zegura. 2003. “Spectral analysis of Internet topologies.” *Proc. IEEE INFOCOM 00 (C)*: 364–74. doi:10.1109/INFCOM.2003.1208688.
- Glasser, Matthew F., Timothy S. Coalson, Emma C. Robinson, Carl D. Hacker, John Harwell, Essa Yacoub, Kamil Ugurbil, et al. 2016. “A multi-modal parcellation of human cerebral cortex.” *Nature* 536 (7615). Nature Publishing Group: 171–78. doi:10.1038/nature18933.
- Glasser, Matthew F., Stamatios N. Sotiropoulos, J. Anthony Wilson, Timothy S. Coalson, Bruce Fischl, Jesper L. Andersson, Junqian Xu, et al. 2013. “The minimal preprocessing pipelines for the Human Connectome Project.” *NeuroImage* 80. Elsevier Inc.: 105–24. doi:10.1016/j.neuroimage.2013.04.127.
- Gordon, Evan M., Timothy O. Laumann, Adrian W. Gilmore, Dillon J. Newbold, Deanna J. Greene, Jeffrey J. Berg, Mario Ortega, et al. 2017. “Precision Functional Mapping of Individual Human Brains.” *Neuron* 95 (4). Elsevier Inc.: 791–807.e7. doi:10.1016/j.neuron.2017.07.011.
- Gratton, Caterina, Timothy O. Laumann, Ashley N. Nielsen, Deanna J. Greene, Evan M. Gordon, Adrian W. Gilmore, Steven M. Nelson, et al. 2018. “Functional Brain Networks Are Dominated by Stable Group and Individual Factors, Not Cognitive or Daily Variation.” *Neuron*. Elsevier Inc., 439–52. doi:10.1016/j.neuron.2018.03.035.
- Griffanti, Ludovica, Gholamreza Salimi-Khorshidi, Christian F. Beckmann, Edward J. Auerbach, Gwenaëlle Douaud, Claire E. Sexton, Eniko Zsoldos, et al. 2014. “ICA-based artefact removal and accelerated fMRI acquisition for improved resting state network imaging.” *NeuroImage* 95: 232–47.

doi:10.1016/j.neuroimage.2014.03.034.

Hiser, Jaryd, and Michael Koenigs. 2018. “The Multifaceted Role of the Ventromedial Prefrontal Cortex in Emotion, Decision Making, Social Cognition, and Psychopathology.” *Biological Psychiatry* 83 (8). Elsevier Inc: 638–47. doi:10.1016/j.biopsych.2017.10.030.

Hubert, Lawrence, and Phipps Arabie. 1985. “Comparing partitions.” *Journal of Classification* 2 (1): 193–218. doi:10.1007/BF01908075.

Kable, Joseph W., and Paul W. Glimcher. 2007. “The neural correlates of subjective value during intertemporal choice.” *Nature Neuroscience* 10 (12): 1625–33.

Kong, Ru, Jingwei Li, Csaba Orban, Mert Rory Sabuncu, Hesheng Liu, Alexander Schaefer, Nanbo Sun, et al. 2018. “Spatial Topography of Individual-Specific Cortical Networks Predicts Human Cognition, Personality and Emotion.” *bioRxiv* 36 (24): 213041. doi:10.1101/213041.

Kragel, Philip A., Michiko Kano, Lukas Van Oudenhove, Huynh Giao Ly, Patrick Dupont, Amandine Rubio, Chantal Delon-Martin, et al. 2018. “Generalizable representations of pain, cognitive control, and negative emotion in medial frontal cortex.” *Nature Neuroscience*. Springer US, 1. doi:10.1038/s41593-017-0051-7.

Laird, A. R., S. B. Eickhoff, K. Li, D. A. Robin, D. C. Glahn, and P. T. Fox. 2009. “Investigating the Functional Heterogeneity of the Default Mode Network Using Coordinate-Based Meta-Analytic Modeling.” *Journal of Neuroscience* 29 (46): 14496–14505. doi:10.1523/JNEUROSCI.4004-09.2009.

Laumann, Timothy O., Evan M. Gordon, Babatunde Adeyemo, Abraham Z. Snyder, Sung Jun Joo, Mei Yen Chen, Adrian W. Gilmore, et al. 2015. “Functional System and Areal Organization of a Highly Sampled Individual Human Brain.” *Neuron* 87 (3). Elsevier Inc.: 658–71. doi:10.1016/j.neuron.2015.06.037.

Levy, I., S. C. Lazzaro, R. B. Rutledge, and P. W. Glimcher. 2011. “Choice from Non-Choice: Predicting Consumer Preferences from Blood Oxygenation Level-Dependent Signals Obtained during Passive Viewing.” *Journal of Neuroscience* 31 (1): 118–25. doi:10.1523/JNEUROSCI.3214-10.2011.

Mackey, Scott, and Michael Petrides. 2014. “Architecture and morphology of the human ventromedial prefrontal cortex.” *European Journal of Neuroscience* 40 (5): 2777–96. doi:10.1111/ejn.12654.

Mueller, Sophia, Danhong Wang, Michael D. Fox, B. T. Thomas Yeo, Jorge Sepulcre, Mert R. Sabuncu, Rebecca Shafee, Jie Lu, and Hesheng Liu. 2013. “Individual Variability in Functional Connectivity Architecture of the Human Brain.” *Neuron* 77 (3). Elsevier Inc.: 586–95. doi:10.1016/j.neuron.2012.12.028.

R Development Core Team. 2018. “R: A language and environment for statistical computing.” Vienna,

Austria, 1. doi:R Foundation for Statistical Computing, Vienna, Austria. ISBN 3-900051-07-0, URL <http://www.R-project.org>.

Salimi-Khorshidi, Gholamreza, Gwenaëlle Douaud, Christian F. Beckmann, Matthew F. Glasser, Ludovica Griffanti, and Stephen M. Smith. 2014. “Automatic denoising of functional MRI data: Combining independent component analysis and hierarchical fusion of classifiers.” *NeuroImage* 90. Elsevier B.V.: 449–68. doi:10.1016/j.neuroimage.2013.11.046.

Tian, Ye, and Andrew Zalesky. 2018. “Characterizing the functional connectivity diversity of the insula cortex: Subregions, diversity curves and behavior.” *NeuroImage*. Elsevier Inc. doi:10.1016/j.neuroimage.2018.08.055.

Tobynne, Sean M., David E. Osher, Samantha W. Michalka, and David C. Somers. 2017. “Sensory-biased attention networks in human lateral frontal cortex revealed by intrinsic functional connectivity.” *NeuroImage* 162 (August). Elsevier Ltd: 362–72. doi:10.1016/j.neuroimage.2017.08.020.

Tobynne, Sean M., David C. Somers, James A. Brissenden, Samantha W. Michalka, Abigail L. Noyce, and David E. Osher. 2018. “Prediction of individualized task activation in sensory modality-selective frontal cortex with ‘connectome fingerprinting’.” *NeuroImage* 183 (August). Elsevier Ltd: 173–85. doi:10.1016/j.neuroimage.2018.08.007.

Van Essen, D. C., K. Ugurbil, E. Auerbach, D. Barch, T. E.J. Behrens, R. Bucholz, A. Chang, et al. 2012. “The Human Connectome Project: A data acquisition perspective.” *NeuroImage* 62 (4): 2222–31. doi:10.1016/j.neuroimage.2012.02.018.

Wager, Tor D., Martin A. Lindquist, Thomas E. Nichols, Hedy Kober, and Jared X. Van Snellenberg. 2009. “Evaluating the consistency and specificity of neuroimaging data using meta-analysis.” *NeuroImage* 45 (1 Suppl). Elsevier Inc.: S210–S221. doi:10.1016/j.neuroimage.2008.10.061.

Yeo, B. T. Thomas, Fenna M. Krienen, Jorge Sepulcre, Mert R. Sabuncu, D. Lashkari, Marisa Hollinshead, Joshua L. Roffman, et al. 2011. “The organization of the human cerebral cortex estimated by intrinsic functional connectivity.” *Journal of Neurophysiology* 106: 1125–65. doi:10.1152/jn.00338.2011.

Zilles, Karl, Nicola Palomero-Gallagher, and Katrin Amunts. 2013. “Development of cortical folding during evolution and ontogeny.” *Trends in Neurosciences* 36 (5). Elsevier Ltd: 275–84. doi:10.1016/j.tins.2013.01.006.